Tensile fracture testing and energy evaluation of a light-cured composite resin

Arakawa, Kazuo
Research Institute for Applied Mechanics, Kyushu University

Kato, Masaru
Research Institute for Applied Mechanics, Kyushu University

Mada, Toshiro
Research Institute for Applied Mechanics, Kyushu University

KYUSHU UNIVERSITY

Tensile fracture testing and energy evaluation of a light-cured composite resin

Kazuo Arakawa[*], Masaru Kato, and Toshio Mada

Research Institute for Applied Mechanics, Kyushu University
6-1 Kasuga-koen, Kasuga-shi, Fukuoka 816-8580, Japan
[*]Corresponding author, E-mail: k.arakaw@riam.kyushu-u.ac.jp
Tel: 81-92-583-7761, Fax: 81-92-593-3947

Abstract

The brittle fracture of a light-cured composite resin used in dental restoration was examined using a high-speed extensometer, consisting of an optical fiber and a position-sensing detector (PSD). Single-edge-cracked specimens for tensile testing were fabricated by packing the composite between two rectangular plates of polymethyl methacrylate (PMMA). In order to study the dynamic effect of brittle fracture and the nonelastic effect of the material, the specimens were pin-loaded with a special jig so that they could split and fly apart in the loading direction after fracture. The flying height and residual deformation of the split specimen were measured to estimate the elastic energy E_e and nonelastic energy E_n, respectively. The fracture energy E_f required to create a new fracture surface was obtained by subtracting E_e and E_n from the external work U_{ex} applied to the specimen. The results showed that the ratio E_f/U_{ex} was about 32% for the composite specimen over a wide range of the fracture load, while it was about 45% for the PMMA specimen. The energy release rate G_f was also estimated using E_f. The results indicated that, although G_f increased with the fracture load, the increasing slope for the composite specimen was smaller than that of the PMMA specimen.

Keywords: Fracture testing; Light-cured resin composite; PMMA; Brittle fracture; Elastic energy; Nonelastic energy; Fracture energy; Energy release rate; High-speed extensometer

1. Introduction

Light-cured composite resins are widely used in dental restoration due to their ease of handling and aesthetic appearance. However, their mechanical strength and resistance to fracture differ markedly from metals traditionally used in restoration, creating a need to develop stronger and more reliable resin composites. In particular, the fracture behavior of composites needs to be carefully assessed to ensure their mechanical reliability. Fracture toughness is usually evaluated in terms of elastic fracture mechanical theory by measuring the crack length and the load or external work applied to a tensile-stressed or bending specimen. Several different types of specimen geometries and experimental methods have been proposed for fracture toughness evaluation of composites [1-4]. However, problems exist in both the light curing procedure as well as the inherent brittleness of the cured material that results from the large content of inorganic powders and fillers, that make it difficult to fabricate standard-sized composite specimens such as are required for fracture toughness evaluation. In addition, most polymers exhibit some nonelastic effects from viscoelastic and plastic deformation [5]. Brittle fracture also causes dynamic or inertia effects when a crack propagates dynamically within the specimen, as is commonly the case [6-25]. These effects also need to be taken into account when evaluating the fracture toughness of brittle materials. Nonetheless, quantitative appraisals of both effects on fracture toughness have seldom been undertaken due to the difficulties inherent in the experimental techniques currently used.

We have explored these issues by measuring brittle fracture in polymers using a tensile loading device we have developed [26-30]. This device consists of a high-speed extensometer that allows quantitative measurements to be made of the static and dynamic displacements near the crack position in single edge-cracked specimens. The elastic energy stored in the specimens was evaluated by determining the flying height of the half specimen following fracture. The dynamic response and residual deformation of the specimen were then measured to evaluate the dynamic and nonelastic effects. The external work applied to the specimen was partitioned into three components: the elastic energy, nonelastic energy, and fracture energy required to create a new fracture surface. The energy release rate for crack propagation was similarly evaluated by

using these parameters and indicated that the dynamic and nonelastic effects play important roles in understanding brittle fracture behavior [26-30].

In this study, we evaluated the proposed experimental procedure using a light-cured resin composite. As outlined above, this material presents a problem in fabricating standard-sized specimens due to both light curing procedures and resulting brittleness. To obviate these difficulties, we fabricated a novel type of single edge-cracked specimen by packing the composite between two rectangular PMMA plates. The nonelastic energy E_n arising from viscoelastic and plastic deformation was then measured using a high-speed extensometer that consisted of an optical fiber and a position-sensing detector (PSD). The elastic energy E_e was calculated from the kinetic energy of the split specimen by measuring the flying height following fracture. The external work U_{ex} was determined from the load and displacement applied to the specimen, and the displacement near the crack was obtained from the PSD. By subtracting E_e and E_n from U_{ex}, we could obtain the fracture energy E_f required to create the new fracture surface. For a fracture surface A_s, the energy release rate was evaluated using $G_f = E_f/A_s$ and correlated with the fracture load of the specimen. This paper discusses the applicability of the experimental method to light-cured resin composites by comparing results with those of reference PMMA specimens.

2. Specimen material and experimental methods

The light-cured resin composite used in this experiment was Clearfil AP-X, supplied by Kuraray Medical, Ltd. This material is a cross-linked acrylic resin composed of about 85 wt% inorganic powders and fillers. It is widely used as a dental restorative material in clinical practice. To overcome the problems of fabricating standard-sized specimens from this material, as outlined above, our specimens had the geometry shown in Fig. 1(a), where the composite was packed between two rectangular plates of PMMA. We used PMMA because it has similar properties to the composite and adheres readily to the resin.

The specimens consisted of two rectangular PMMA plates (Sumipex E), 3 mm thick, 20 mm wide, and 90 mm long. Clearfil Tri-S Bond bonding agent (Kuraray Medical, Ltd.) was applied to the end surfaces of the plates and irradiated using a Morita Jetlite 3000 light unit to

cure the agent. The two plates were directionally aligned using two frames on a transparent

5 mm thick PMMA plate with a 10 mm clearance gap, and the composite was packed into the

gap and irradiated with the light.

To prevent specimen curvature following the curing, the composite was irradiated eight

times alternately from the top and bottom (four times of 5 s duration and four times of 10 s

duration) followed by a further 10 s upon removal of the frames. The surface of the composite

was then ground and polished flat. Each specimen was stored for 24 hrs in air at room

temperature. The PMMA specimen shown in Fig. 1(b) was made to provide a comparison with

the composite specimen.

The experimental procedure is illustrated in Fig. 2. The lower portion of the specimen was

clamped rigidly and the upper part tightly confined with steel plate grips and a pin-shaped bolt

and nut to satisfy the symmetry requirements. The specimen was then loaded at the pin.

Fracture loading of the specimens was initiated at sharp pre-cracks of differing lengths ranging

from 2 to 7 mm made by tapping a fresh razor blade into a pre-machined saw-cut on the

specimen edge. A load was then introduced using a special loading jig consisting of four steel

bars, as shown in Fig. 3. The shape of the jig allowed the specimen to split and fly apart in the

loading direction after fracture. The flying height was recorded with a thin flexible paper pipe

(0.3 g) inserted between the bars. The pipe rose with the split specimen (30 g) and stopped at the

highest position attained by the uppermost part of the specimen due to friction between the pipe

and the bars. This provided an estimate of the elastic energy contained in the specimen. In this

study, the elastic energy in the jig was disregarded due to its far greater stiffness compared to

the specimens. All specimens were tested under a displacement-controlled condition using a

tensile testing machine, with tests performed at room temperature and at a constant crosshead

rate of 1 mm/min.

Figure 2 also shows the configuration used to determine the displacement measurements

of the loading point and the region beneath the pre-crack position, *i.e.*, the centerline of the

specimen. The loading point displacement was measured with the tensile testing machine,

while the displacement near the pre-crack was determined from the optical fiber and PSD

(SiTek Electro Optics) [26-30]. In this experiment, the fiber was attached at a point 2 mm from

the pre-crack to avoid any damage arising from dynamic crack propagation. A laser diode provided the light source and an amplifier and digital wave memory recorded the output signals from the PSD. The PSD is an optoelectronic device that converts an incident light spot into continuous position data due to the lateral photo effect, and has a frequency response of 100 kHz. As a consequence, it allowed both static and dynamic displacements to be measured.

3. Experimental results

Figure 4 shows a typical load P versus displacement δ diagram for a composite specimen determined from the tensile testing machine. As shown in the figure, P increased almost linearly with δ, but then dropped abruptly at P_c and δ_c, the critical values related to dynamic fracture initiation in the specimen. The P–δ diagram was partitioned into three regions, as discussed in subsequent sections.

To examine the residual displacement after fracture, the relationship between δ' near the pre-crack and the time t was recorded as a sampling rate $\Delta t = 1$ µs. Figure 5 shows that following fracture δ' exhibited a damped oscillation behavior that fluctuated about δ'_n. This indicates that there was a residual displacement during the oscillation owing to nonelastic deformation of the material. δ'_n was ascertained first by determining the midpoints of the initial two oscillations. The intersection of a straight line between these two points and the line of the curve falling from δ'_c was taken as the residual displacement δ'_n of the split specimen. Then δ'_n was corrected to obtain the value δ_n at the centerline of the specimen by using the position of the optical fiber on the specimen. Figure 6 shows δ_n as a function of the critical load P_c. Since δ_n for the two materials increased with P_c, this implies that δ_n increased with the critical load of the specimen. Further, there was a difference between the two values of δ_n obtained from the composite and from the PMMA specimen for a given P_c.

Figure 7 shows the flying height H_e of the split specimen as a function of the critical load P_c. Although the data are scattered, H_e for the composite and PMMA specimens increased with P_c so as to imply that an increase in fracture load generated elastic energy in the specimen and hence an increase in flying height.

4. Definition of fracture energy

The nonlinearity in the P–δ diagram for both materials is not significant (see Fig. 4). Hence, the external work U_{ex} applied to a specimen can be determined as:

$$U_{ex} = P_c \delta_c / 2. \tag{1}$$

This analysis assumes that U_{ex} can be partitioned into the three regions shown in Fig. 4:

$$U_{ex} = E_f + E_e + E_n, \tag{2}$$

where E_f is the fracture energy created for half the new surfaces, E_e is the specimen's elastic energy, and E_n is the nonelastic energy arising from the specimen's viscoelastic and plastic deformation [26-30].

Assumptions were made in determining E_e and E_n. First, we assumed that E_e was converted into the kinetic energy following specimen fracture. Second, we assumed that the change from P_c to δ_e or δ_n was elastic since the material's viscosity can be neglected during dynamic crack propagation (see Fig. 4) [22, 23]. Hence:

$$\frac{E_e}{U_{ex}} = \frac{(\delta_e - \delta_n)}{\delta_c}, \qquad \frac{E_n}{U_{ex}} = \frac{\delta_n}{\delta_c} \tag{3}$$

5. Evaluation of fracture energies

The nonelastic energy E_n was evaluated using Eq. (3) and the nonelastic displacement δ_n determined for both the composite and PMMA specimens (see Fig. 6). Figure 8 shows the ratio E_n/U_{ex} as a function of the critical load P_c. E_n/U_{ex} of the composite specimen increased almost linearly with P_c. It reached about 38% in the region of small P_c, and about 57% in the region of large P_c, while E_n/U_{ex} for the PMMA specimen remained almost constant at 40% over a wide P_c range.

From the flying height H_e of the split specimen after fracture (see Fig. 7), the elastic energy E_e in the specimen could be evaluated as:

$$E_e = mgH_e, \tag{4}$$

where m is the total mass of half the specimen, loading pin, grip, and paper pipe, and g is the gravitational acceleration. Figure 8 also shows the ratio E_e/U_{ex} as a function of the critical load P_c. The value of E_e/U_{ex} for the composite specimen was about 27% in the region of small P_c,

and about 12% in the region of large P_c, with E_e/U_{ex} for the PMMA specimen remaining almost constant at 14% over a wide P_c range. In this analysis, we were unable to make a quantitative evaluation of the energy loss caused by elastic wave generation from the crack tip and the friction between the loading jig and the paper pipe or split specimen; this energy loss was disregarded. Hence, the elastic energy determined from Eq. (4) may have been underestimated.

The fracture energy E_f was evaluated from Eq. (2) by substituting the elastic and nonelastic energies. Figure 9 shows the energy ratio E_f/U_{ex} as a function of the critical load P_c. Although there was a scattering of E_f/U_{ex} data for the composite specimen, the value remained almost constant at 32% over a wide P_c range. A similar situation existed for the PMMA specimen, with E_f/U_{ex} remaining nearly constant at 45%. This suggests that E_f/U_{ex} was not strongly influenced by the fracture conditions in terms of parameters such as P_c, δ_c, or U_{ex}.

The energy release rate G_f was estimated from:

$$G_f = E_f/A_s \tag{5}$$

where A_s is half the area of the total fracture surface. Figure 10 shows G_f as a function of P_c. G_f increased in both materials with P_c, although the slope for the composite specimen was less than that of the PMMA specimen. This difference supports the validity of both the present testing method and of the specimen geometry employed, particularly given the difference in fracture behavior of the two materials. It is our intention to explore this effect in more detail in our future work by investigating the crack velocity during crack propagation, given that the energy release rate also depends on the velocity.

6. Conclusions

The fracture behavior of a light-cured resin composite was examined using single-edge-cracked tensile specimens fabricated by packing the composite between two rectangular PMMA plates. From the load and displacement relationship, the external work U_{ex} applied to the specimen was used to establish the elastic energy E_e, nonelastic energy E_n due to viscoelastic and plastic deformation, and fracture energy E_f involved in creating a new fracture surface A_s. The energy release rate was then estimated from $G_f = E_f/A_s$. The energy ratios E_n/U_{ex},

E_e/U_{ex}, E_f/U_{ex}, and G_f for the composite specimen were then correlated with the fracture load P_c, and compared with those for PMMA specimens. The results showed the following.

(1) E_e/U_{ex} for the composite specimen was about 27% in the region of small P_c, and about 12% in the region of large P_c, while E_e/U_{ex} for the PMMA specimen remained almost constant at 14% over a wide P_c range.

(2) E_n/U_{ex} for the composite specimen was about 38% in the region of small P_c, and about 57% in the region of large P_c, while E_n/U_{ex} for the PMMA specimen remained almost constant at 40% over a wide P_c range.

(3) E_f/U_{ex} for the composite specimen was about 32% over a wide range of P_c, but was about 45% for the PMMA specimen.

(4) G_f for both materials increased with P_c, but the slope of the composite specimen was less than that of the PMMA specimen.

Acknowledgments

References

[1] R.E. Kovarik, J.W. Ergle, C.W. Fairhurst, Effects of specimen geometry on the measurement of fracture toughness, Dent. Mater. 7 (1991) 166-169.

[2] Y. Higo, D. Damri, S. Nunomura, K. Kumada, N. Sawa, K. Hanaoka, T. Teranaka, T. Iwamoto, The fracture toughness characteristics of three dental composite resins, Biomed. Mater. Engng. 1 (1991) 223-231.

[3] D.J. Indrani, W.D. Cook, F. Televantos, M.J. Tyas, K. Harcourt, Fracture toughness of water-aged resin composite restorative materials, Dent. Mater. 11 (1995) 201-207.

[4] L.A. Knobloch, R.E. Kerby, R. Seghi, J.S. Berlin, N. Clelland, Fracture toughness of packable and conventional composite materials, J. Prosthet. Dent. 88-3 (2002) 307-313.

[5]   J.G. Williams, Fracture Mechanics of Polymers, Ellis Horwood Limited, Chichester, 1984.

[6]   A.S. Kobayashi, Handbook on Experimental Mechanics, Prentice-Hall, Inc., Englewood Cliffs, New Jersey, 1987.

[7]   K. Ravi-Chandar, Experimental challenges in the investigation of dynamic fracture of brittle materials, Bouchaud, et al. (Eds) Physical Aspects of Fracture, E. Kluwer Academic Publisher, Netherlands, 2001, pp. 323-342

[8]   T. Kobayashi, J.W. Dally, Relation between crack velocity and the stress intensity factor in birefringent polymers, G.T. Hahn, M.F. Kanninen (Eds.), Fast Fracture and Crack Arrest, ASTM STP, vol. 627, 1977, pp. 257-273.

[9]   J.W. Dally, A. Shukla, Energy loss in Homalite 100 during crack propagation and arrest, Eng. Fract. Mech. 13 (1980) 807-817.

[10] A. Shukla, H. Nigam, A note on the stress intensity factor and crack velocity relationship for Homalite 100, Eng. Fract. Mech. 25 (1986) 91-102.

[11] A.S. Kobayashi, M. Ramulu, M.S. Dadkhah, K.-H.Yang, B.S.J. Kang, Dynamic fracture toughness, Int. J. Fract. 30 (1986) 275-285.

[12] J.W. Dally, R.K. Agarwal, R.J. Sanford, A study of hysteresis in the K_{ID}-$\dot{a}$ relation, Exp. Mech. 30 (1990) 177-183.

[13] P.S. Theocaris, G.A. Papadopoulos, Elasto-dynamic forms of caustics for running cracks under constant velocity, Eng. Fract. Mech. 13 (1980) 683-698.

[14] J.F. Kalthoff, On some current problems in experimental fracture dynamics, in: W.G. Knauss (Ed.), Workshop on Dynamic Fracture, California Institute of Technology, Pasadena, 1983, pp.11-35.

[15] W.G. Knauss, K. Ravi-Chandar, Some basic problems in stress wave dominated fracture, Int. J. Fract. 27 (1985) 127-143.

[16] K. Takahashi, K. Arakawa, Dependence of crack acceleration on the dynamic stress intensity factor in polymers, Exp. Mech. 27 (1987) 195-200.

[17] F.G. Katsamanis, C.G. Delides, Fracture surface energy measurements of PMMA: a new experimental approach, Journal of Physics D: Applied Physics 21 (1988) 79-861.

[18] S. Suzuki, H. Homma, R. Kusaka, Pulsed holographic microscopy as a measurement method of dynamic fracture toughness for fast propagating cracks, J. Mech. Phys. Solids 36-6 (1988) 631-653.

[19] T. Nishioka, T. Murakami, H. Uchiyama, K. Sakakura, H. Kittaka, Specimen size effects on dynamic crack propagation and arrest in DCB specimens, Eng. Fract. Mech. 39 (1991) 757-767.

[20] K. Arakawa, K. Takahashi, Relationships between fracture parameters and fracture surface roughness of brittle polymers, Int. J. Fract. 48 (1991) 103-114.

[21] K. Arakawa, K. Takahashi, Branching of a fast crack in polymers, Int. J. Fract. 48 (1991) 245-259.

[22] K. Arakawa, D. Nagoh, K. Takahashi, Crack velocity and acceleration effects on the dynamic stress intensity factor in polymers, Int. J. Fract. 83 (1997) 305-313.

[23] K. Arakawa, D. Nagoh, K. Takahashi, Dynamic crack propagation and unloading behavior of brittle polymers, Int. J. Fract. 96 (1999) 347-360 .

[24] K. Arakawa, T. Mada, K. Takahashi, Correlations among dynamic stress intensity factor, crack velocity and acceleration in brittle fracture, Int. J. Fract. 105 (2000) 311-320.

[25] K. Arakawa, T. Mada, Unsteady dynamic crack propagation in a brittle polymer, Exp. Mech. 47 (2007) 609-615.

[26] K. Arakawa, T. Mada, Measuring fracture energy in a brittle polymeric material, Exp. Mech. 46 (2006) 347-353.

[27] K. Arakawa, T. Mada, Measuring fracture energy in a brittle polymeric material, Application of a high-speed optical extensometer, Exp. Mech. 47 (2007) 211-216.

[28] K. Arakawa, T. Mada, S. D. Park, M. Todo, Tensile fracture behavior of a biodegradable polymer, poly(lactic acid), Polym. Test 25 (2006) 628-634.

[29] K. Arakawa, T. Mada, M. Todo, J. Takahashi, S. Ooka, Impact tensile fracture testing of a brittle polymer, Polym. Test 25 (2006) 1095-1100.

[30] K. Arakawa, T. Mada, M. Todo, J. Takahashi, S. Ooka, Effect of rubber particle size on the impact tensile fracture behavior of MBS resin with a bimodal particle size distribution, J. Mater. Sci. 42 (2007) 8700-8706.

Figure Captions

Fig. 1 Specimen geometries: (a) composite resin, (b) PMMA.

Fig. 2 Experimental setup.

Fig. 3 Loading jigs used for the static test.

Fig. 4 Load P versus displacement δ.

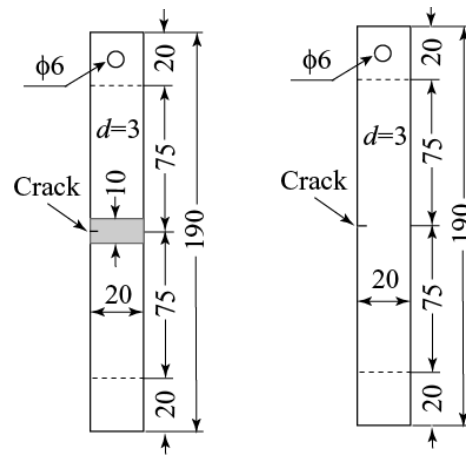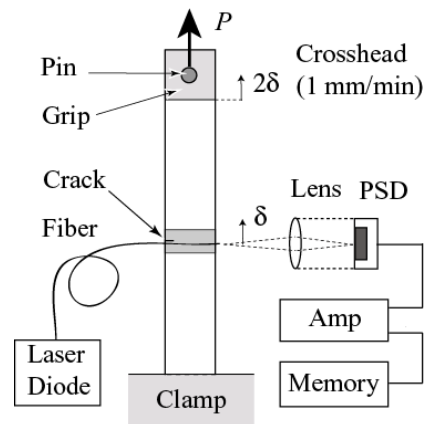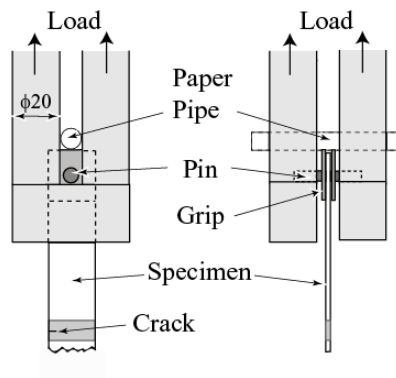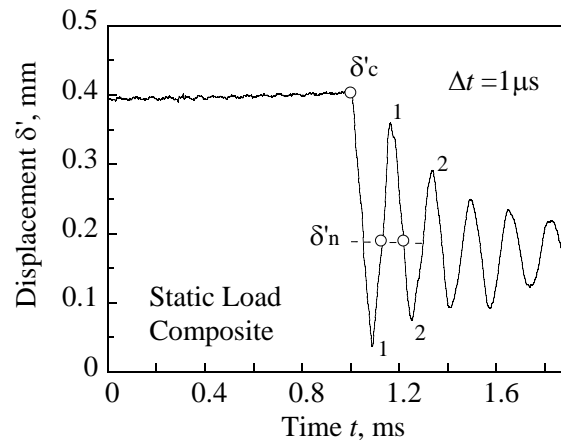Fig. 5 Displacement δ' versus time t.
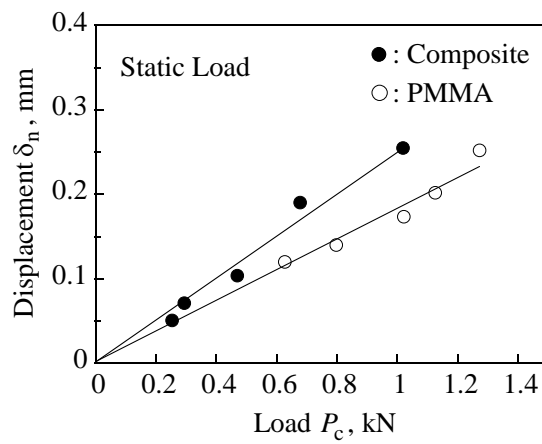
Fig. 6 Residual displacement δ_n versus fracture load P_c.
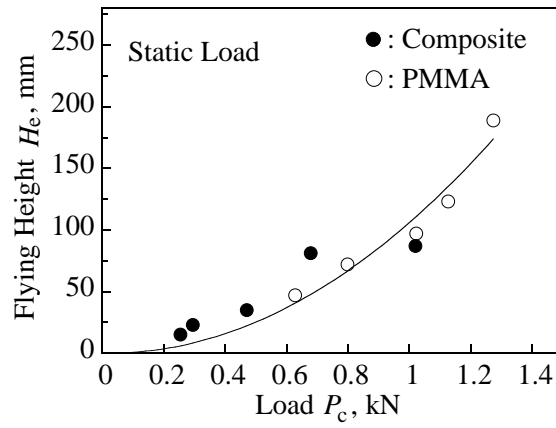
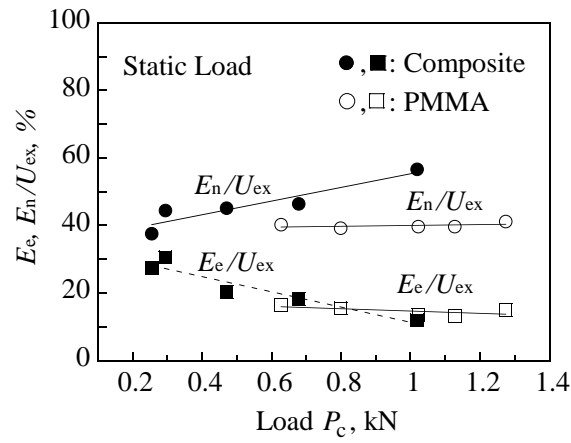Fig. 7 Flying height H_e versus fracture load P_c.

Fig. 8 Energy ratios E_e/U_{ex} and E_n/U_{ex} versus fracture load P_c.

Fig. 9 Energy ratio E_f/U_{ex} versus fracture load P_c.

Fig. 10 Energy release rate G_f versus fracture load P_c.

(a) composite resin   (b) PMMA

Fig. 1 Specimen geometries.

Fig. 2 Experimental setup.

Fig. 3 Loading jigs used for the static test.

Fig. 4 Load P versus displacement δ.

Fig. 5 Displacement δ' versus time t.

Fig. 6 Residual displacement δ_n versus fracture load P_c.

Fig. 7 Flying height H_e versus fracture load P_c.

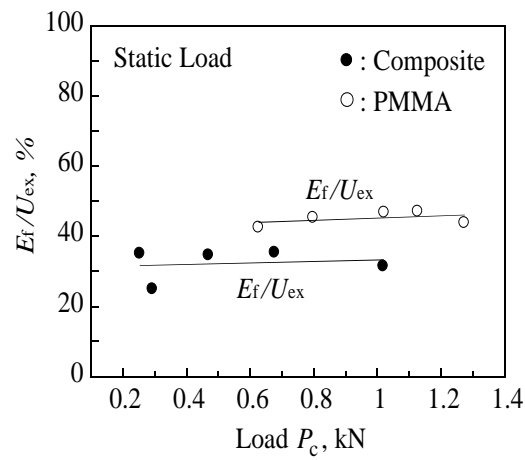Fig. 8 Energy ratios E_e/U_{ex} and E_n/U_{ex} versus fracture load P_c

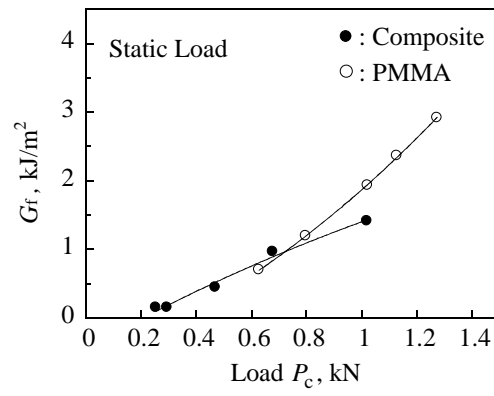Fig. 9 Energy ratio E_f/U_{ex} versus fracture load P_c.

Fig. 10 Energy release rate G_f versus fracture load P_c.